Journal of Computational Physics 228 (2009) 6107–6118

Contents lists available at ScienceDirect

Journal of Computational Physics

journal homepage: www.elsevier.com/locate/jcp

# Implementation of diffuse reflection boundary conditions in a thermal lattice Boltzmann model with flux limiters

Victor Sofonea *

*Center for Fundamental and Advanced Technical Research, Romanian Academy, Bd. Mihai Viteazul 24, RO-300223 Timişoara, Romania*

ARTICLE INFO

*Article history:*
Received 17 September 2008
Received in revised form 2 April 2009
Accepted 9 May 2009
Available online 18 May 2009

*PACS:*
47.11.–j
51.10.+y

*Keywords:*
Lattice Boltzmann
Boundary conditions
Flux limiter
Couette flow

ABSTRACT

We discuss three new implementation versions of diffuse reflection boundary conditions in a thermal lattice Boltzmann model. Their accuracy is investigated in the case of Couette flow by considering the slip regime. The best results are recovered with versions 2 and 3, which rely on outgoing fluxes to express the particle distribution functions in the ghost nodes outside the flow domain. Version 2 is found to be more economical since it involves no interpolation procedure. This version was thereafter used to investigate the temperature profile in Couette flow for various values of Prandtl number, as well as the capability of the thermal LB model to capture the Knudsen minimum in Poiseuille flow.



## 1. Introduction

It is well known that the continuum hypothesis is no longer valid when the Knudsen number $\mathrm{Kn} = \lambda/L$, defined as the ratio between the mean free path $\lambda$ of fluid particles and the characteristic size $L$ of the flow domain, becomes noticeable ($\mathrm{Kn} > 0.01$). For such cases, encountered in both micro-scale and rarefied gas flow, the use of Navier–Stokes–Fourier equations, as well as of the traditional techniques of computational fluid dynamics (CFD), becomes questionable [1–6]. Lattice Boltzmann (LB) models provide a promising alternative to CFD, as well as to molecular dynamics (MD) or direct simulation Monte Carlo (DSMC) models. LB models are derived from the Boltzmann equation using a simplified version of the collision term, as well as an appropriate discretisation of the phase space [7–13]. The interest for the use of LB models to investigate micro-scale flows is growing constantly [14–35], especially because traditional models currently used to investigate fluid physics at non-negligible values of Kn (MD and DSMC) need huge computing resources that can easily exceed the capacity of today's supercomputers [1,2,4–6].

Implementation of boundary conditions (BC) is crucial to enable proper use of LB models for the investigation of micro-scale flow. Velocity slip and rarefaction phenomena were first evidentiated by LB simulations in the pioneering works of Nie et al. [14], as well as of Lim et al. [15]. Various implementations of BC were later considered in the literature [16–35] in order to fit the specific numerical schemes used to solve the partial derivative equations that control the evolution of the

* Tel.: +40 256 491 816; fax: +40 256 403 700.
*E-mail address:* sofonea@acad-tim.tm.edu.ro
*URL:* http://www.acad-tim.tm.edu.ro/~sofonea

0021-9991/$ - see front matter © 2009 Elsevier Inc. All rights reserved.
doi:10.1016/j.jcp.2009.05.009

distribution functions in the LB models. Many of these implementations are based on the diffuse reflection concept, which dates back to the time of Maxwell and Smoluchowski [36,37].

The implementation of diffuse reflection boundary conditions in the two-dimensional finite difference lattice Boltzmann model with multiple speeds and variable temperature, developed by Watari and Tsutahara [38], as done in Ref. [26], requires the use of the first order upwind finite difference scheme in the lattice nodes adjacent to the walls of the flow domain, even if higher order numerical schemes may be considered in the bulk nodes [29]. Although this implementation of BC was successfully used [26,29,30] to capture the main characteristics of micro-channel flow (velocity slip and temperature jump near the walls, as well as the thermal creep phenomenon), the accuracy of the simulation results near the flow domain walls still needs to be improved [29].

The purpose of this paper is to introduce new versions of the diffuse reflection boundary conditions for the two-dimensional LB model of Watari and Tsutahara [38], as well as to investigate their accuracy. Although we restrict ourselves to a particular model where second order flux limiter schemes [29,30,39–42] are considered to enhance numerical accuracy in the bulk nodes while preserving the stability in the presence of density gradients [30,43], the implementation of our boundary conditions may be easily conducted in other finite difference LB models as well. The paper is organized as follows. For convenience, the multispeed model with variable temperature of Watari and Tsutahara, as well as the flux limiter numerical scheme are briefly described in Section 2. The existing implementation of diffuse reflection boundary conditions for this model, as well as three new versions are introduced in Section 3. In Section 4, their accuracy is investigated in the case of Couette and Poiseuille flow.

## 2. Description of the lattice Boltzmann model with variable temperature and flux limiters

The thermal LB model of Watari and Tsutahara (WT) involves a set of 33 nondimensionalized velocities [38]

$$\mathrm{e}_{00}=0,\quad \mathrm{e}_{ki}=\left[\cos\frac{\pi(i-1)}{4},\sin\frac{\pi(i-1)}{4}\right]c_k\quad (k=1,\ldots 4,\ i=1,\ldots 8) \tag{1}$$

The values of the speeds $c_k\in\{1.0,\,1.92,\,2.99,\,4.49\}$ were determined in [38] to ensure the stability of this model within the largest possible temperature range $(0.4\leqslant\theta\leqslant 1.6)$. The corresponding distribution functions $f_{00}=f_{00}(\mathbf{x},t), f_{ki}=f_{ki}(\mathbf{x},t)$ are defined in the nodes $\mathbf{x}$ of a square lattice. The local fluid density $n$, the velocity $\mathbf{u}$ and the temperature $\theta$ are determined from these distribution functions, as follows [38]:

$$n=\sum_{ki}f_{ki} \tag{2}$$

$$nu_\alpha=\sum_{ki}f_{ki}e_{ki\alpha} \tag{3}$$

$$n\left(\theta+\frac{u^2}{2}\right)=\frac{1}{2}\sum_{ki}f_{ki}c_k^2 \tag{4}$$

The distribution functions in the thermal model of Watari and Tsutahara evolve according to the following equation (in nondimensionalized form)

$$\partial_t f_{ki}+\mathbf{e}_{ki}\cdot\nabla f_{ki}=-\frac{1}{\tau}[f_{ki}-f_{ki}^{eq}] \tag{5}$$

where the equilibrium distribution functions

$$f_{ki}^{eq}=f_{ki}^{eq}(\mathbf{x},t)=nF_ks_{ki} \tag{6}$$

are expressed using the series expansion $s_{ki}=s_{ki}(\theta,\mathbf{u})$ up to fourth order [38] with respect to the Cartesian components $u_\alpha(\alpha=1,2)$ of the fluid velocity (summation over repeated Greek indices is understood):

$$s_{ki}=\left(1-\frac{u^2}{2\theta}+\frac{u^4}{8\theta^2}\right)+\frac{1}{\theta}\left(1-\frac{u^2}{2\theta}\right)e_{ki\xi}u_\xi+\frac{1}{2\theta^2}\left(1-\frac{u^2}{2\theta}\right)e_{ki\xi}e_{ki\eta}u_\xi u_\eta+\frac{1}{6\theta^3}e_{ki\xi}e_{ki\eta}e_{ki\zeta}u_\xi u_\eta u_\zeta+\frac{1}{24\theta^4}e_{ki\xi}e_{ki\eta}e_{ki\zeta}e_{ki\chi}u_\xi u_\eta u_\zeta u_\chi \tag{7}$$

The weight factors $F_k=F_k(\theta)$ in Eq. (6) depend on the local temperature $\theta=\theta(\mathbf{x},t)$ and the speeds $c_k, k=1,\ldots 4$:

$$F_k=\frac{1}{c_k^2\left(c_k^2-c_{\{k+1\}}^2\right)\left(c_k^2-c_{\{k+2\}}^2\right)\left(c_k^2-c_{\{k+3\}}^2\right)}\times\Big[48\theta^4-6\left(c_{\{k+1\}}^2+c_{\{k+2\}}^2+c_{\{k+3\}}^2\right)\theta^3 +\left(c_{\{k+1\}}^2c_{\{k+2\}}^2+c_{\{k+2\}}^2c_{\{k+3\}}^2+c_{\{k+3\}}^2c_{\{k+1\}}^2\right)\theta^2-c_{\{k+1\}}^2c_{\{k+2\}}^2c_{\{k+3\}}^2\theta/4\Big] \tag{8}$$

$$F_0=1-8(F_1+F_2+F_3+F_4) \tag{9}$$

Here we used the notation ($l = 1,2,3$)

$$\{k+l\} = \begin{cases} k+l, & k+l \leqslant 4 \\ k+l-4, & k+l > 4 \end{cases} \tag{10}$$

Although the WT model needs more computing resources because of the relatively large number of distribution functions when compared to other lattice Boltzmann models with variable temperature, like the internal energy density distribution function (IEDDF) model [44–47], one should stress the fact that all observable fields (density, velocity and temperature) are derived by WT from the same distribution function, as in standard kinetic theory. The WT strategy may be useful to derive also higher order LB models by further expanding the Maxwell-Boltzmann distribution function to higher orders, as suggested in [48].

In order to control the Knudsen number during computer simulations, the non-dimensionalized relaxation time $\tau$ in Eq. (5) is expressed as [26]

$$\tau = \frac{\Lambda}{n\bar{c}} \tag{11}$$

where $\Lambda$ is a constant, $n$ is the local particle density introduced in Eq. (2) and

$$\bar{c} = \frac{\sum_{k=1}^{4} c_k \sum_{i=1}^{8} f_{ki}}{f_0 + \sum_{k=1}^{4}\sum_{i=1}^{8} f_{ki}} \tag{12}$$

is the local average speed of fluid particles. In the sequel, we adopt the value $\Lambda = 10^6$, which corresponds to a flow domain whose characteristic size is $\mathcal{L} = 10^{-6}$ m [26]. As discussed in [26], the value of Knudsen number is given by

$$\mathrm{Kn} = \frac{\Lambda}{n} \tag{13}$$

Since the nondimensionalized speeds $c_k$ of the thermal LB model are no longer related to the lattice spacing $\delta s$ and the time step $\delta t$, as in the standard (collision – streaming) LB models [11,12], finite difference schemes need to be used to evolve the distribution functions in each lattice node [38]. The use of finite difference schemes in LB model, first proposed in [49], allows for more freedom in the discretization of the phase space. Higher order schemes based on flux limiters proved to be efficient and stable during computer simulations done using this model [29,30,43]. These schemes are briefly outlined below.

Let $f_{ki}^{n,j} = f_{ki}(\mathbf{x}_j, t)$ be the value of the distribution function $f_{ki}$ at time $t$ in the node $\mathbf{x}_j$ on the characteristic line along the direction $i$ (for convenience, the characteristic line for direction $i = 2$ is shown in Fig. 1). The updated value $f_{ki}^{n+1,j} = f_{ki}(\mathbf{x}_j, t+\delta t)$ of the distribution function $f_{ki}^{n,j}$ at time $t + \delta t$ in the node $\mathbf{x}_j$ is computed using two fluxes

$$f_{ki}^{n+1,j} = f_{ki}^{n,j} - \frac{c_k \delta t}{A_i \delta s}\left[\mathcal{F}_{ki}^{n,j+1/2} - \mathcal{F}_{ki}^{n,j-1/2}\right] - \frac{\delta t}{\tau}\left[f_{ki}^{n,j} - f_{ki}^{eq,n,j}\right] \tag{14}$$

where

$$A_i = \begin{cases} 1, & i \in \{1,3,5,7\} \\ \sqrt{2}, & i \in \{2,4,6,8\} \end{cases} \tag{15}$$

The outgoing and incoming fluxes in node $j$ along the direction $i$ are

$$\mathcal{F}_{ki}^{n,j+1/2} = f_{ki}^{n,j} + \frac{1}{2}\left(1 - \frac{c_k \delta t}{A_i \delta s}\right)\left[f_{ki}^{n,j+1} - f_{ki}^{n,j}\right]\Psi(\Theta_{ki}^{n,j}) \tag{16}$$

$$\mathcal{F}_{ki}^{n,j-1/2} = \mathcal{F}_{ki}^{n,(j-1)+1/2} \tag{17}$$

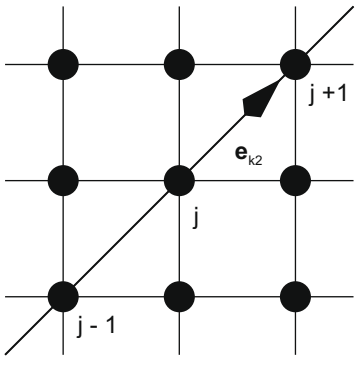


**Fig. 1.** Characteristic line on the square lattice ($i = 2$).

where $\Psi(\Theta_{ki}^{n,j})$ is the flux limiter and

$$\Theta_{ki}^{n,j} = \frac{f_{ki}^{n,j} - f_{ki}^{n,j-1}}{f_{ki}^{n,j+1} - f_{ki}^{n,j}} \tag{18}$$

is the smoothness function [39,40]. From the wide choice of flux limiters in the literature [39–41], which all work well with LB models, we adopt the Monitorized Central Difference (MCD) flux limiter given by

$$\Psi\left(\Theta_{ki}^{n,j}\right) = \begin{cases} 0, & \Theta_{ki}^{n,j} \leqslant 0 \\ 2\Theta_{ki}^{n,j}, & 0 \leqslant \Theta_{ki}^{n,j} \leqslant \frac{1}{3} \\ \left(1 + \Theta_{ki}^{n,j}\right)/2, & \frac{1}{3} \leqslant \Theta_{ki}^{n,j} \leqslant 3 \\ 2, & 3 \leqslant \Theta_{ki}^{n,j} \end{cases} \tag{19}$$

## 3. Diffuse reflection boundary conditions

Application of the updating rule (14) in the bulk nodes of the lattice is straightforward. The same holds for lattice nodes where periodic boundary conditions apply. Special attention should be paid when applying the updating rule (14) in the boundary nodes located near the walls of the flow domain. Let us consider a rectangular flow domain bounded by two vertical walls. According to the *diffuse reflection* concept [1,2,17,22,26,36,37], the distribution functions of the particles directing to the wall mix themselves (i.e., *thermalize*) in wall nodes as a result of particle-wall interaction and become Maxwellian before getting reflected into the fluid (see Fig. 2, which refers to the left wall of constant temperature $\theta_{wl}$ and velocity $\mathbf{u}_{wl}$). More precisely, the distribution functions whose corresponding velocities point normal to the wall mix separately from the distribution functions corresponding to velocities orientated along the diagonals of the square lattice.

A procedure, which relies on interpolation to define the values of the distribution functions in the ghost nodes outside the wall, was already introduced in the LB model of Watari and Tsutahara [26,29,30]. For convenience, this implementation of the diffuse reflection boundary conditions that we call *version 0* from now on, is described below. A drawback of this version is the use of the first order upwind finite difference scheme to update the distribution functions in the boundary nodes near the walls, even if flux limiter schemes may be easily used in the bulk nodes [29]. For this reason, three new and more elaborated versions of the diffuse reflection boundary conditions will be further introduced in this Section to allow the use of flux limiter schemes in the boundary nodes, too.

### 3.1. Version 0

We refer to the left channel wall in Fig. 2, since the right wall is handled in a similar manner. The wall is located half lattice spacing between the ghost nodes and the fluid nodes. Let the indices $(j, l)$ fix the position of a node into the lattice.

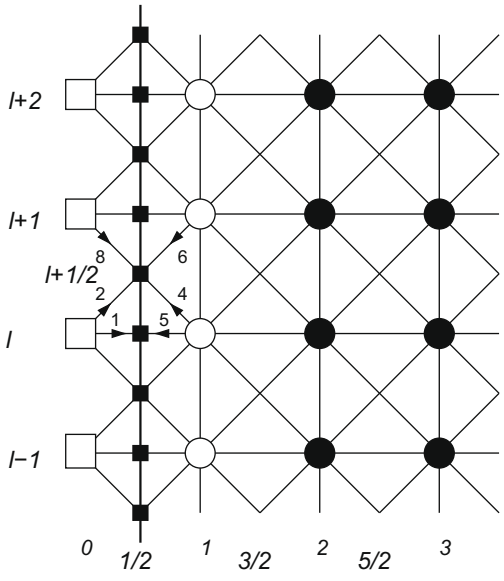


**Fig. 2.** Diffuse reflection boundary conditions: □ - ghost nodes, ○ – boundary nodes, • – bulk nodes, ■ - wall nodes where the distribution functions $f_{ki}(k = 1, \ldots 4, i = 1, 2, 8)$ follow the Maxwell distribution law.

The black squares $(j = 1/2, l)$ and $(j = 1/2, l + 1/2), l = 0, 1, \ldots$, denote the mixing nodes on the wall. The corresponding (unknown) values of the particle number density are $n_{wl}^{1/2,l}$ and $n_{wl}^{1/2,l+1/2}$, respectively. Because of particle-wall interactions, the distribution function of fluid particles reflected by the walls becomes Maxwellian. The values of the distribution functions $f_{k1}^{0,l}, f_{k2}^{0,l}$ and $f_{k8}^{0,l+1}, (l = 0, 1, \ldots)$, defined in the ghost nodes $(j = 0, l)$ outside the wall need to be computed in order to use the updating rule (14) for the distribution functions in the lattice nodes $(j = 1, l)$ located near the wall. For these nodes, the MCD scheme is reduced to the first order upwind scheme by setting the corresponding value of the flux limiter to zero.

Following the discretization of the velocity space, in the LB model the Maxwellian distribution function is replaced by the set of equilibrium distribution functions, Eq. (6), and the distribution functions of reflected particles may be calculated in wall nodes using an interpolation procedure. This gives $(k = 1, \ldots 4)$:

$$\frac{f_{k1}^{0,l} + f_{k1}^{1,l}}{F_k(\theta_{wl}) s_{k1}(\theta_{wl}, \mathbf{u}_{wl})} = 2 n_{wl}^{1/2,l} \tag{20}$$

$$\frac{f_{k2}^{0,l} + f_{k2}^{1,l+1}}{F_k(\theta_{wl}) s_{k2}(\theta_{wl}, \mathbf{u}_{wl})} = \frac{f_{k8}^{0,l+1} + f_{k8}^{1,l}}{F_k(\theta_{wl}) s_{k8}(\theta_{wl}, \mathbf{u}_{wl})} = 2 n_{wl}^{1/2,l+1/2} \tag{21}$$

Eqs. (20), (21), together with the requirements that there is no mass flux perpendicular to the wall in the mixing nodes:

$$\sum_k c_k f_{k5}^{1,l} = \sum_k c_k f_{k1}^{0,l} \tag{22}$$

$$\sum_k c_k \left[ f_{k4}^{1,l} + f_{k6}^{1,l+1} \right] = \sum_k c_k \left[ f_{k2}^{0,l} + f_{k8}^{0,l+1} \right] \tag{23}$$

may be solved to get the values of the distribution functions in the ghost nodes (0,l) and (0,l+1) after each time step.

### 3.2. Version 1

In this version, the interpolation procedure is rejected. We simply assume that the distribution functions in the ghost nodes are identical to the corresponding distribution functions in the wall nodes. Since the reflected distribution functions in the wall nodes are Maxwellian, this assumption means

$$\begin{aligned} f_{k1}^{0,l} &= n_{wl}^{1/2,l} F_k(\theta_{wl}) s_{k1}(\theta_{wl}, \mathbf{u}_{wl}) \\ f_{k2}^{0,l} &= n_{wl}^{1/2,l+1/2} F_k(\theta_{wl}) s_{k2}(\theta_{wl}, \mathbf{u}_{wl}) \\ f_{k8}^{0,l+1} &= n_{wl}^{1/2,l+1/2} F_k(\theta_{wl}) s_{k8}(\theta_{wl}, \mathbf{u}_{wl}) \end{aligned} \tag{24}$$

After replacing the expressions (24) of the ghost distribution functions in the conservation Eqs. (22,23), we get the values of the fluid density in the wall nodes:

$$n_{wl}^{1/2,l} = \frac{\sum_k c_k f_{k5}^{1,l}}{\sum_k c_k F_k(\theta_{wl}) s_{k1}(\theta_{wl}, \mathbf{u}_{wl})} \tag{25}$$

$$n_{wl}^{1/2,l+1/2} = \frac{\sum_k c_k \left[ f_{k4}^{1,l} + f_{k6}^{1,l+1} \right]}{\sum_k c_k F_k(\theta_{wl}) \left[ s_{k2}(\theta_{wl}, \mathbf{u}_{wl}) + s_{k8}(\theta_{wl}, \mathbf{u}_{wl}) \right]} \tag{26}$$

Eq. (24) are then used to get the values of the distribution functions in the ghost nodes.

### 3.3. Version 2

The distribution functions in the ghost nodes are still considered identical to the reflected functions defined in the wall nodes and thus, Eq. (24) hold also in this version. However, the distribution functions defined in the boundary nodes ($f_{k5}^{1,l}, f_{k4}^{1,l}$ and $f_{k6}^{1,l+1}$) that appear in the conservation Eqs. (22), (23) are replaced by the corresponding outgoing fluxes ($\mathcal{F}_{k5}^{1/2,l}, \mathcal{F}_{k4}^{1/2,l+1/2}$ and $\mathcal{F}_{k6}^{1/2,l+1/2}$) defined in the wall nodes:

$$\sum_k c_k \mathcal{F}_{k5}^{1/2,l} = \sum_k c_k f_{k1}^{0,l} \tag{27}$$

$$\sum_k c_k \left[ \mathcal{F}_{k4}^{1/2,l+1/2} + \mathcal{F}_{k6}^{1/2,l+1/2} \right] = \sum_k c_k \left[ f_{k2}^{0,l} + f_{k8}^{0,l+1} \right] \tag{28}$$

The outgoing fluxes in the equations above are computed according to Eq. (16), where the value of the smoothness function is assumed to equal the unit value. In this case, most of the flux limiters in the literature, including MCD [39–41] also equal the unit value. Consequently, we get

$$\begin{aligned}
\mathcal{F}_{k5}^{1/2,l} &= f_{k5}^{1,l} + \frac{1}{2}\left(1 - \frac{c_k\delta t}{A_5\delta s}\right)\left[f_{k5}^{1,l} - f_{k5}^{2,l}\right] \\
\mathcal{F}_{k4}^{1/2,l+1/2} &= f_{k4}^{1,l} + \frac{1}{2}\left(1 - \frac{c_k\delta t}{A_4\delta s}\right)\left[f_{k4}^{1,l} - f_{k4}^{2,l-1}\right] \\
\mathcal{F}_{k6}^{1/2,l+1/2} &= f_{k6}^{1,l+1} + \frac{1}{2}\left(1 - \frac{c_k\delta t}{A_6\delta s}\right)\left[f_{k6}^{1,l+1} - f_{k6}^{2,l+2}\right]
\end{aligned} \tag{29}$$

The values of the fluid particle density in the wall nodes are recovered from Eq. (24) and the conservation Eqs. (27), (28):

$$n_{wl}^{1/2,l} = \frac{\sum_k c_k \mathcal{F}_{k5}^{1/2,l}}{\sum_k c_k F_k(\theta_{wl}) s_{k1}(\theta_{wl}, \mathbf{u}_{wl})} \tag{30}$$

$$n_{wl}^{1/2,l+1/2} = \frac{\sum_k c_k \left[\mathcal{F}_{k4}^{1/2,l+1/2} + \mathcal{F}_{k6}^{1/2,l+1/2}\right]}{\sum_k c_k F_k(\theta_{wl})[s_{k2}(\theta_{wl}, \mathbf{u}_{wl}) + s_{k8}(\theta_{wl}, \mathbf{u}_{wl})]} \tag{31}$$

As in the previous version, Eq. (24) are finally used to get the values of the distribution functions in the ghost nodes.

### 3.4. Version 3

The interpolation procedure defined by Eqs. (20), (21) is kept in this version, while the distribution functions defined in the ghost nodes ($f_{k1}^{0,l}, f_{k2}^{0,l}$ and $f_{k8}^{0,l+1}$), which appear in the conservation Eqs. (27), (28) used in the previous version are replaced by the incoming fluxes $\mathcal{F}_{k1}^{1/2,l}, \mathcal{F}_{k2}^{1/2,l+1/2}$ and $\mathcal{F}_{k8}^{1/2,l+1/2}$:

$$\begin{aligned}
&\sum_k c_k \mathcal{F}_{k5}^{1/2,l} = \sum_k c_k \mathcal{F}_{k1}^{1/2,l} \\
&\sum_k c_k \left[\mathcal{F}_{k4}^{1/2,l+1/2} + \mathcal{F}_{k6}^{1/2,l+1/2}\right] = \sum_k c_k \left[\mathcal{F}_{k2}^{1/2,l+1/2} + \mathcal{F}_{k8}^{1/2,l+1/2}\right]
\end{aligned} \tag{32}$$

The incoming fluxes are computed after setting the smoothness function to the unit value:

$$\begin{aligned}
\mathcal{F}_{k1}^{1/2,l} &= f_{k1}^{0,l} + \frac{1}{2}\left(1 - \frac{c_k\delta t}{A_1\delta s}\right)\left[f_{k1}^{1,l} - f_{k1}^{0,l}\right] \\
\mathcal{F}_{k2}^{1/2,l+1/2} &= f_{k2}^{0,l} + \frac{1}{2}\left(1 - \frac{c_k\delta t}{A_2\delta s}\right)\left[f_{k2}^{1,l+1} - f_{k2}^{0,l}\right] \\
\mathcal{F}_{k8}^{1/2,l+1/2} &= f_{k8}^{0,l+1} + \frac{1}{2}\left(1 - \frac{c_k\delta t}{A_8\delta s}\right)\left[f_{k8}^{1,l} - f_{k8}^{0,l+1}\right]
\end{aligned} \tag{33}$$

After application of the interpolation procedure (20), (21), the incoming fluxes become

$$\begin{aligned}
\mathcal{F}_{k1}^{1/2,l} &= \left(1 + \frac{c_k\delta t}{A_1\delta s}\right) n_{wl}^{1/2,l} F_k(\theta_{wl}) s_{k1}(\theta_{wl}, \mathbf{u}_{wl}) - \frac{c_k\delta t}{A_1\delta s} f_{k1}^{1,l} \\
\mathcal{F}_{k2}^{1/2,l+1/2} &= \left(1 + \frac{c_k\delta t}{A_2\delta s}\right) n_{wl}^{1/2,l+1/2} F_k(\theta_{wl}) s_{k2}(\theta_{wl}, \mathbf{u}_{wl}) - \frac{c_k\delta t}{A_2\delta s} f_{k2}^{1,l+1} \\
\mathcal{F}_{k8}^{1/2,l+1/2} &= \left(1 + \frac{c_k\delta t}{A_8\delta s}\right) n_{wl}^{1/2,l+1/2} F_k(\theta_{wl}) s_{k8}(\theta_{wl}, \mathbf{u}_{wl}) - \frac{c_k\delta t}{A_8\delta s} f_{k8}^{1,l}
\end{aligned} \tag{34}$$

The values of the fluid particle density in the wall nodes are retrieved after replacing (29) and (34) in the conservation Eq. (32):

$$\begin{aligned}
n_{wl}^{1/2} &= \frac{\sum_k c_k \left[\frac{c_k\delta t}{A_1\delta s} f_{k1}^{1,l} + f_{k5}^{1,l} + \frac{1}{2}\left(1 - \frac{c_k\delta t}{A_5\delta s}\right)\left(f_{k5}^{1,l} - f_{k5}^{2,l}\right)\right]}{\sum_k c_k \left(1 + \frac{c_k\delta t}{A_1\delta s}\right) F_k(\theta_{wl}) s_{k1}(\theta_{wl}, \mathbf{u}_{wl})} \\
n_{wl}^{1/2} &= \frac{\sum_k c_k \left[\frac{c_k\delta t}{A_2\delta s} f_{k2}^{1,l+1} + f_{k6}^{1,l+1} + \frac{1}{2}\left(1 - \frac{c_k\delta t}{A_6\delta s}\right)\left(f_{k6}^{1,l+1} - f_{k6}^{2,l+2}\right)\right]}{\sum_k c_k \left[\left(1 + \frac{c_k\delta t}{A_2\delta s}\right) F_k(\theta_{wl}) s_{k2}(\theta_{wl}, \mathbf{u}_{wl}) + \left(1 + \frac{c_k\delta t}{A_8\delta s}\right) F_k(\theta_{wl}) s_{k8}(\theta_{wl}, \mathbf{u}_{wl})\right]} \\
&\quad + \frac{\sum_k c_k \left[\frac{c_k\delta t}{A_8\delta s} f_{k8}^{1,l} + f_{k4}^{1,l} + \frac{1}{2}\left(1 - \frac{c_k\delta t}{A_4\delta s}\right)\left(f_{k4}^{1,l} - f_{k4}^{2,l-1}\right)\right]}{\sum_k c_k \left[\left(1 + \frac{c_k\delta t}{A_2\delta s}\right) F_k(\theta_{wl}) s_{k2}(\theta_{wl}, \mathbf{u}_{wl}) + \left(1 + \frac{c_k\delta t}{A_8\delta s}\right) F_k(\theta_{wl}) s_{k8}(\theta_{wl}, \mathbf{u}_{wl})\right]}
\end{aligned} \tag{35}$$

These values allow us to compute the values of the distribution functions in ths ghost nodes, according to the interpolation procedure (21).

## 4. Computer results

### 4.1. Accuracy of the four implementation versions of the diffuse reflection boundary conditions

Simulation of Couette flow was used to test the new implementation versions of the diffuse reflection boundary conditions. A two-dimensional fluid system was placed between two vertical walls located at $x = -L/2$ and $x = L/2$, where $L = 1$ is the non-dimensionalized channel width. Periodic boundary conditions were applied in the $y$ direction. The left and right walls move in opposite directions with velocities $\mathbf{u}_{wl} = -\mathbf{u}_w$ and $\mathbf{u}_{wr} = \mathbf{u}_w$, respectively. The wall speed was set to $u_w = 0.1$. The corresponding wall temperatures are $\theta_{wl}$ and $\theta_{wr}$.

We restrict ourselves to Couette flow in the *slip flow regime* (Kn < 0.1), when the spatial extension of the Knudsen layer is still negligible and the velocity profile across the channel is well approximated by a linear one [1,2,4,5]. In this case, analytical solutions for the vertical component $u(x)$ of the fluid velocity and the temperature $\theta(x)$ in the normal direction to the channel walls are available [26]:

$$u(x) = Ax + B \tag{36}$$

$$\theta(x) = Cx^2 + Dx + E \tag{37}$$

where the coefficients

$$A = \frac{u_{wr} - u_{wl}}{1 + 2\mathrm{Kn}} \tag{38}$$

$$B = \frac{u_{wr} + u_{wl}}{2} \tag{39}$$

$$C = -\frac{\eta}{2\kappa}A^2 \tag{40}$$

$$D = \frac{\theta_{wr} - \theta_{wl}}{1 + 2\mathrm{Kn}} \tag{41}$$

$$E = \frac{\eta}{8\kappa}A^2(1 + 4h\mathrm{Kn}) + \frac{\theta_{wr} + \theta_{wl}}{2} \tag{42}$$

are expressed using the dynamic fluid viscosity $\eta = n\theta\tau$ and the thermal conducibility $\kappa = 2n\theta\tau$ [38]. For the thermal model of Watari and Tsutahara, the constant $h$ in Eq. (42) has the value $(\gamma = 2)$

$$h = \frac{2\gamma}{\gamma + 1}\frac{1}{\mathrm{Pr}} = \frac{4}{3} \tag{43}$$

where

$$\mathrm{Pr} = \frac{2\eta}{\kappa} = 1 \tag{44}$$

is the Prandtl number.

Temperature jump and slip velocity are specific to micro-scale flow when the Knudsen number is no longer negligible. For Couette flow with $\mathrm{u}_{wr} = -\mathrm{u}_{wl} = \mathrm{u}_w$ and $\theta_{wr} = \theta_{wl} = \theta_w$, the temperature jump and the slip velocity at the walls are given by [26]

$$u^{slip} = u_w + u(-L/2) = u_w - u(L/2) = u_w\frac{2\zeta\mathrm{Kn}}{(1 + 2\zeta\mathrm{Kn})} \tag{45}$$

$$\theta^{jump} = \theta(-L/2) - \theta_w = \theta(L/2) - \theta_w = u_w^2\mathrm{Pr}\frac{h\mathrm{Kn}}{(1 + 2\mathrm{Kn})^2} \tag{46}$$

where $\zeta = 1.15$ is a correction factor [26].

Typical profiles of velocity and temperature in Couette flow are shown in Fig. 3 for three values of Kn. These profiles were recovered on a lattice with $N = 100$ nodes in the horizontal direction and three nodes in the vertical direction by using *version 2* of the diffuse reflection boundary conditions, as well as the MCD flux limiter scheme. The slip velocity and the temperature jump increase with Kn, as expected. The MCD flux limiter scheme, which is of second order with respect to the lattice spacing $\delta s = L/N$, is preferred against the much simpler first order upwind scheme because of the lower numerical dissipation [29,41,42]. This is justified in Fig. 4, where simulation results recovered for Kn = 0.001 with the first order upwind scheme, as well as with the MCD flux limiter scheme, are compared to theoretical results, Eq. (37), for two values of $N$. Higher fluid temperature values are observed in the middle of the channel when using the first order upwind scheme. These unphysical values are due to numerical dissipation, which plagues the first order upwind scheme, and are still observed when decreasing the lattice spacing $\delta s$ by increasing the number of lattice nodes $N$ per unit length. Even if other second order finite difference schemes like the space centered scheme, the second order upwind scheme, Lax-Wendroff or Lax-Friedrichs, may be considered to reduce numerical dissipation, it is known that these schemes become unstable in the presence of density gradients which arise, e.g., in multiphase systems [41]. For this reason, the new versions of the diffuse reflection

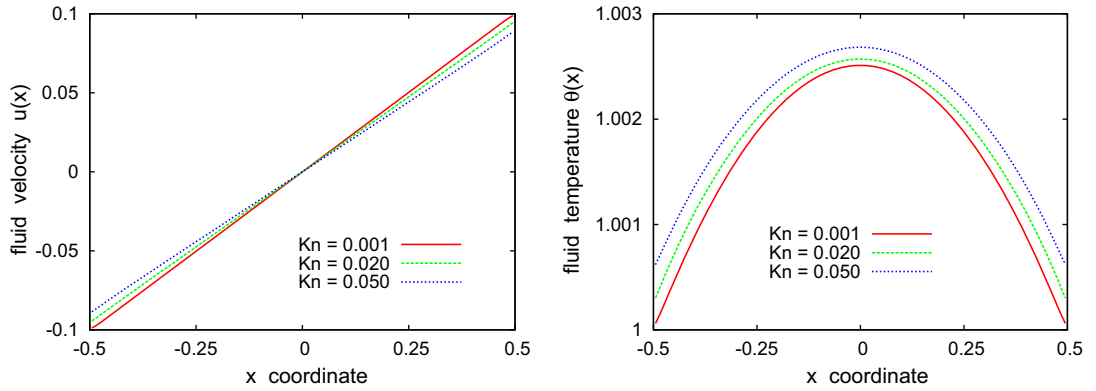


**Fig. 3.** Velocity and temperature profiles across the channel in Couette flow, recovered using *version 2* of the diffuse reflection boundary conditions.

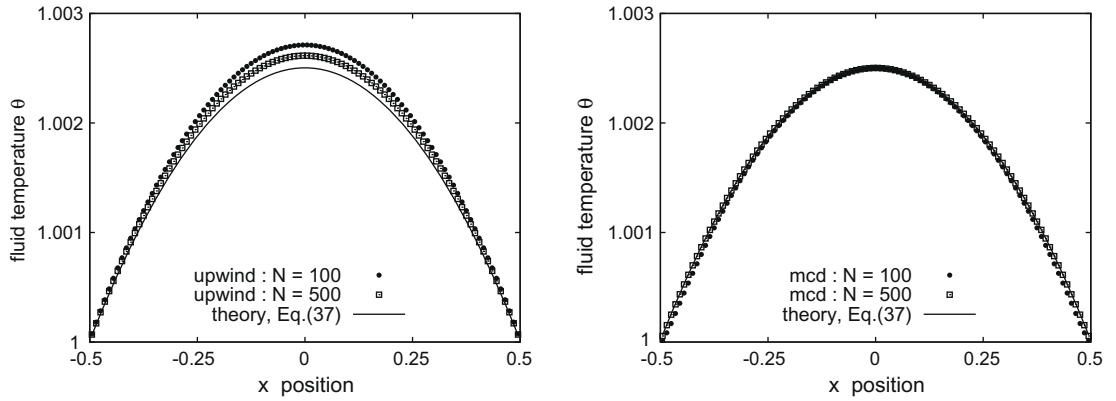


**Fig. 4.** Temperature profiles across the channel in Couette flow, recovered using *version 0* of the diffuse reflection boundary conditions and two finite difference schemes (*left:* first order upwind; *right:* second order MCD flux limiter).

boundary conditions, introduced in this paper, were especially designed to allow the incorporation of flux limiter schemes in the lattice nodes adjacent to the flow domain walls.

To compare the accuracy of the four implementation versions of the diffuse reflection boundary conditions discussed in Section 3, we used the same lattice spacing $\delta s = L/N(N = 100)$ for all computer runs and plotted in Fig. 5 the dependence of the velocity slip $u^{slip}$ at the left channel wall, as well as of the corresponding temperature jump $\theta^{jump}$, with respect to the Knudsen number. Since the fluid velocity and temperature values are defined in the nodes of a discrete lattice, a second order

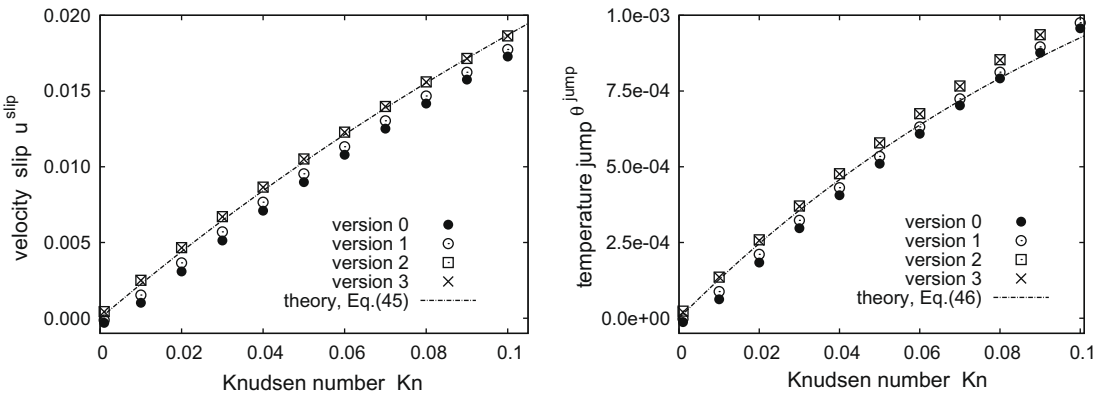


**Fig. 5.** Effect of Knudsen number on the velocity slip and temperature jump near the left channel wall in Couette flow, as recovered with various implementations of the diffuse reflection boundary conditions ($\delta s = 0.01$).

extrapolation technique was used in order to get the values $\theta(-L/2), u(-L/2)$ of the fluid temperature and velocity on the left channel wall, which appear in Eqs. (45) and (46).

As seen in Fig. 5, comparison between LB simulation results and the analytical solutions (45) and (46) reveals that versions 2 and 3 of the diffuse reflection boundary conditions, which give quite identical results, are generally more accurate than the results recovered when using versions 0 and 1 in the slip flow regime. Moreover, versions 0 and 1 give unphysical (negative) values of the velocity slip $u^{slip}$ and the temperature jump $\theta^{jump}$ for very small values of Kn. According to Fig. 6, these unphysical values are specific to larger values of the lattice spacing $\delta s$. As the lattice spacing becomes smaller, the numerical accuracy of the four versions improves significantly and both quantities (velocity slip and temperature jump) evolve towards the corresponding values computed in accordance to Eqs. (45) and (46). However, in Fig. 6 one can easily see that version 0 of the diffuse reflection boundary conditions still exhibits the largest numerical errors, regardless the value of the lattice spacing $\delta s$.

For a quantitative estimation of numerical errors introduced by the four versions of the diffuse reflection boundary conditions, we compared the corresponding transversal velocity and temperature profiles for Kn = 0.001 to the analytical results, Eqs. (36) and (37). Let $x_j, j = 1, 2, \ldots N$ be the coordinates of the lattice nodes along a transversal section of the channel and $u_j, \theta_j$ be the corresponding values of the local fluid velocity and temperature, recovered using the LB method. Following quantities provide global estimations of the accuracy of velocity and temperature profiles, respectively:

$$E_{vel} = \delta s \sum_{j=1}^{N} |u_j - u(x_j)| \tag{47}$$

$$E_{temp} = \delta s \sum_{j=1}^{N} |\theta_j - \theta(x_j)| \tag{48}$$

where $u(x_j), \theta(x_j)$ are the corresponding values of the velocity and temperature in the lattice node $j$ along the transversal section, as computed using the analytical solutions, Eqs. (36) and (37). As seen in Fig. 7, the accuracy of the simulation results is significantly higher when using versions 2 or 3 of the diffuse reflection boundary conditions. The accuracy scales with $(\delta s)^2$, as expected because the MCD flux limiter scheme is of second order.

### 4.2. Control of Prandtl number

A current problem concerning the lattice Boltzmann models with variable temperature is related to the achievement of various values of the Prandtl number Pr during computer simulations. The value Pr=1 is uniquely defined in single relaxation time LB models like the thermal model of Watari and Tsutahara since both transport coefficients (viscosity $\eta$ and heat conducibility $\kappa$) are proportional to the relaxation time $\tau$. LB models that allow to control the value of Pr were recently proposed in the literature and rely on various schemes like multiple relaxation times or adjusted collision terms [33,50–57]. In the case of the LB model used in this paper, the control of Pr may be achieved by introducing a force term $I_{ki}$ [43] in the evolution Eq. (5):

$$\partial_t f_{ki} + \mathbf{e}_{ki} \cdot \nabla f_{ki} = -\frac{1}{\tau}\left[f_{ki} - f_{ki}^{eq}\right] + I_{ki} \tag{49}$$

The force term

$$I_{ki} = -\frac{1}{2n\theta^2}[\nabla \cdot (2qn\theta\tau\nabla\theta)][-2\theta + (\mathbf{e}_{ki} - \mathbf{u})^2]f_{ki}^{eq} \tag{50}$$

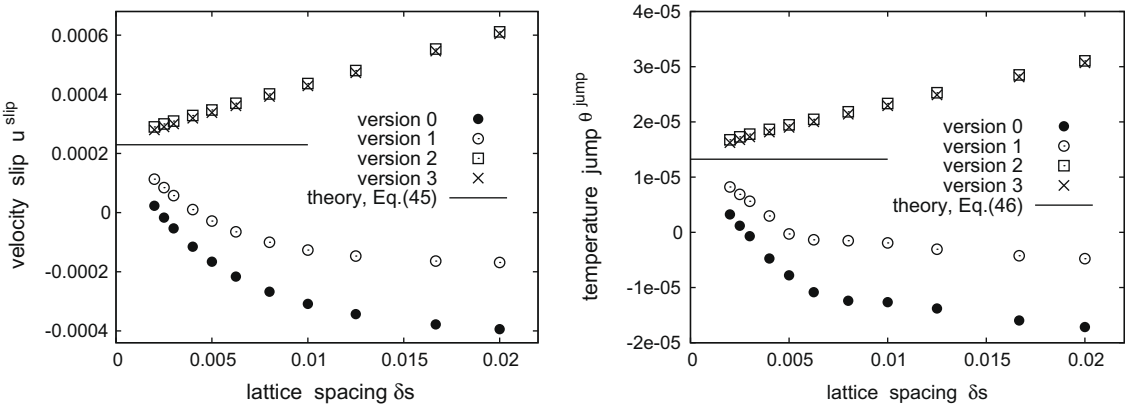


**Fig. 6.** Dependence of the velocity slip $u^{slip}$ and the temperature jump $\theta^{jump}$ on the lattice spacing $\delta s$, for Kn = 0.001.

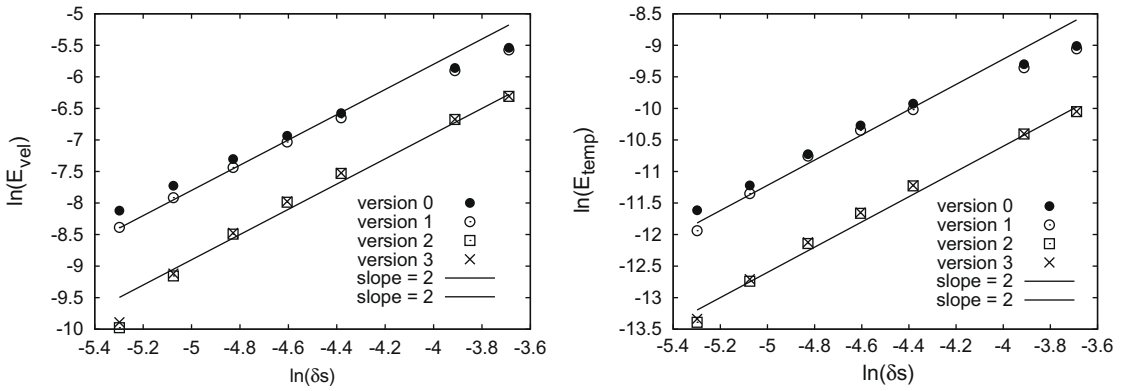


**Fig. 7.** Dependence of $E_{vel}$ and $E_{temp}$ defined in Eqs. (47) and (48) vs. lattice spacing $\delta s$, for Kn = 0.001.

changes the value of the heat conducibility in the energy equation by a factor $(q+1)$, from $\kappa = 2n\theta\tau$ to $\kappa = 2(q+1)n\theta\tau$ [43]. Consequently, the Prandtl number changes from Pr=1 to $\mathrm{Pr} = 1/(1+q)$.

We performed a series of simulations using version 2 of our diffuse reflection boundary conditions in order to check its compatibility with the force term $I_{ki}$ introduced above. For this purpose, we considered the thermal Couette flow between two vertical walls of different temperatures $\theta_{wl} = 1 - \Delta/2, \theta_{wr} = 1 + \Delta/2, \Delta = 0.006666$. The walls move in opposite directions with velocities $\mathbf{u}_{wl} = -\mathbf{u}_w$ and $\mathbf{u}_{wr} = \mathbf{u}_w$, as previously. The simulations were done on a lattice with $N = 100$ nodes in the normal direction to the walls. Fig. 8 shows the temperature profiles normalized to $\Delta$, for various values of Pr, when Kn=0.001. These temperature profiles agree to the theoretical profiles derived according to Eq. (37).

### 4.3. Evidence of Knudsen minimum in poiseuille flow

Poiseuille flow driven by a constant force along the channel was also considered to further check the improved boundary conditions introduced in this paper. A key test is the evidence of the so-called Knudsen minimum, i.e., the minimum value of the mass flow rate plotted as a function of Knudsen number Kn [1,2]. This minimun has been experimentally observed long time ago [58] and reported only recently in lattice Boltzmann simulations [21,25,30,59–61].

We carried a series of LB simulations for various values of Knudsen number Kn using version 2 of our diffuse reflection boundary conditions on the same lattice with $100 \times 3$ nodes ($\delta s = 0.01$) that was used in Section 4.1. Both walls were at rest ($\mathbf{u}_{wl} = \mathbf{u}_{wr} = 0$) and had the same temperature $\theta_w = 1$. The fluid was subjected to a constant acceleration $a = 0.001$ in the vertical direction. Following Ref. [59], the resulted fluid flow rates in the stationary state

$$\mathcal{Q}(\mathrm{Kn}) = \int_{-L/2}^{L/2} n(x,y)u_y(x,y)dx \tag{51}$$

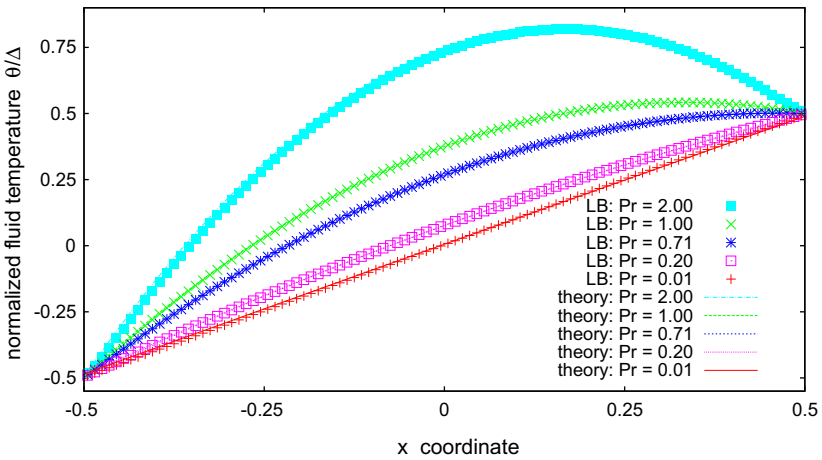


**Fig. 8.** Dependence of the normalized temperature profile $\theta/\Delta$ across the channel in Couette flow, for various values of Prandtl number Pr.

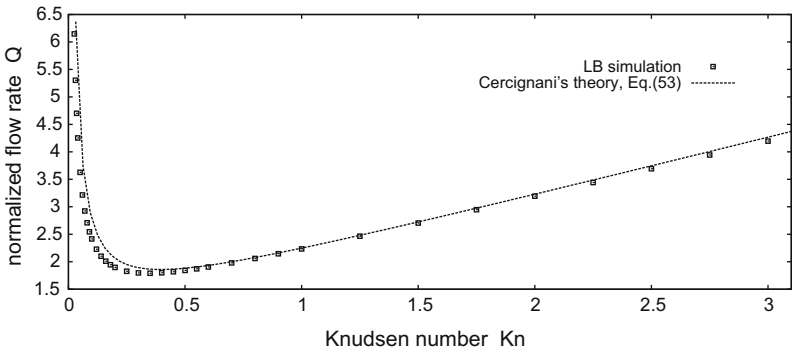


**Fig. 9.** Dependence of the normalized flow rate Q in Poiseuille flow vs. Knudsen number Kn.

were normalized by the factor

$$\mathcal{Q}_0 = \frac{aL^2}{\bar{c}} \tag{52}$$

The normalized flow rates $\mathrm{Q}(\mathrm{Kn}) = \mathcal{Q}(\mathrm{Kn})/\mathcal{Q}_0$ are plotted in Fig. 9 and agree well to the analytical result of Cercignani [62]

$$\mathrm{Q} = \frac{1}{6\mathrm{Kn}} + s + (2s^2 - 1)\mathrm{Kn}, \quad s = 1.01615 \tag{53}$$

even beyond the slip flow regime (Kn > 0.1). Note that the minimum flow rate is recovered for Kn = 0.35 in our simulations, while the minimum value of the expression (53) is located at $\mathrm{Kn} \simeq 0.394$.

## 5. Conclusion

Three new implementation versions of the diffuse reflection boundary conditions were introduced for the two-dimensional LB model with variable temperature of Watari and Tsutahara [38] in order to allow to use second order flux limiter schemes in the lattice nodes adjacent to the flow domain walls. The accuracy of the new implementations was tested in the case of the slip flow regime of Couette flow (Kn<0.1). For small Kn and large $\delta s$, unphysical (negative) values of the velocity slip and temperature jump are observed when using versions 0 and 1 of the diffuse reflection boundary conditions. Analysis of computer results show that the newly introduced versions 2 and 3 of the diffuse reflection boundary conditions, which involve outgoing fluxes instead of particle distribution functions, give the best results. Version 2 involves no interpolation procedure to determine the distribution functions in the ghost nodes outside the flow domain and hence is more economical. This version was thereafter used to investigate the temperature profile in Couette flow for various values of Prandtl number, as well as the capabiliy of the thermal LB model to capture the Knudsen minimum in Poiseuille flow. Application of this version of diffuse reflection boundary conditions to higher-order lattice Boltzmann models introduced recently [48] will be the subject of further work.

## Acknowledgments

This work was supported by Romanian Academy Grant GAR 301/2007.

## References

[1] G.E. Karniadakis, A. Beskok, N. Aluru, Microflows and Nanoflows: Fundamentals and Simulation, Springer, Berlin, 2005.
[2] C. Shen, Rarefied Gas Dynamics: Fundamentals, Simulations and Micro Flows, Springer, Berlin, 2005.
[3] P. Tabeling, Introduction to Microfluidics, Oxford University Press, Oxford, 2005.
[4] M. Gad-el-Hak (Ed.), MEMS Handbook, Introduction and Fundamentals, vol. I, CRC Taylor and Francis, Boca Raton, 2006.
[5] M. Gad-el-Haq, The fluid mechanics of microdevices, Journal of Fluids Engineering 121 (1999) 5.
[6] J.M. Reese, M.A. Gallis, D.A. Lockerby, New directions in fluid dynamics: non-equilibrium aerodynamic and microsystem flows, Philosophical Transactions of the Royal Society Series A 361 (2003) 2967.
[7] R. Benzi, S. Succi, M. Vergassola, The lattice Boltzmann equation: theory and applications, Physics Reports 222 (1992) 145.
[8] D.H. Rothman, S. Zaleski, Lattice Gas Cellular Automata: Simple Models of Complex Hydrodynamics, Cambridge University Press, Cambridge, 1997.
[9] B. Chopard, M. Droz, Cellular Automata Modeling of Physical Systems, Cambridge University Press, Cambridge, 1998.
[10] S. Chen, G.D. Doolen, Lattice Boltzmann method for fluid flow, Annual Review of Fluid Mechanics 30 (1998) 329.
[11] D.A. Wolf-Gladrow, Lattice Gas Cellular Automata and Lattice Boltzmann Models, Springer, Berlin, 2000.
[12] S. Succi, The Lattice Boltzmann Equation for Fluid Dynamics and Beyond, Clarendon Press, Oxford, 2001.
[13] M.C. Sukop, D.T. Thorne, Lattice Boltzmann Modeling: An Introduction for Geoscientists and Engineers, Springer, Berlin, 2006.
[14] X. Nie, G.D. Doolen, S. Chen, Lattice Boltzmann simulation of fluid flows in MEMS, Journal of Statistical Physics 107 (2002) 279.
[15] C.Y. Lim, C. Shu, X.D. Niu, Y.T. Chew, Application of lattice Boltzmann method to simulate microchannel flows, Physics of Fluids 14 (2002) 2299.
[16] S. Succi, Mesoscopic modeling of slip motion at fluid-solid interfaces with heterogeneous catalysis, Physical Review Letters 89 (2002) 064502.

[17] S. Ansumali, I.V. Karlin, Kinetic boundary conditions in the lattice Boltzmann method, Physical Review E 66 (2002) 026311.
[18] B. Li, D. Kwok, Discrete Boltzmann equation for microfluidics, Physical Review Letters 90 (2003) 124502.
[19] X.D. Niu, C. Shu, Y.T. Chew, A lattice Boltzmann BGK model for simulation of micro flows, Europhysics Letters 67 (2004) 600.
[20] T. Lee, C. Lin, Rarefaction and compressibility effects of the lattice-Boltzmann-equation method in a gas microchannel, Physical Review E 71 (2005) 046706.
[21] Y. Zhang, R. Qin, D.R. Emerson, Lattice Boltzmann simulation of rarefied gas flows in microchannels, Physical Review E 71 (2005) 047702.
[22] V. Sofonea, R.F. Sekerka, Boundary conditions for the upwind finite difference lattice Boltzmann model: evidence of slip velocity in micro-channel flow, Journal of Computational Physics 207 (2005) 639.
[23] M. Sbragaglia, S. Succi, Analytical calculation of slip flow in lattice Boltzmann models with kinetic boundary conditions, Physics of Fluids 17 (2005) 093602.
[24] S. Ansumali, I. Karlin, Consistent lattice Boltzmann method, Physical Review Letters 97 (2005) 260605.
[25] F. Toschi, S. Succi, Lattice Boltzmann method at finite Knudsen numbers, Europhysics Letters 69 (2005) 549.
[26] V. Sofonea, R.F. Sekerka, Diffuse-reflection boundary conditions for a thermal lattice Boltzmann model in two dimensions: evidence of temperature jump and slip velocity in microchannels, Physical Review E 71 (2005) 066709.
[27] Z. Guo, T.S. Zhao, Y. Shi, Physical symmetry, spatial accuracy and relaxation time of the lattice Boltzmann equation for microgas flows, Journal of Applied Physics 99 (2006) 074903.
[28] R. Benzi, L. Biferale, M. Sbragaglia, S. Succi, F. Toschi, Mesoscopic two-phase model for describing apparent slip in micro-channel flows, Europhysics Letters 74 (2006) 651.
[29] V. Sofonea, Lattice Boltzmann approach to thermal transpiration, Physical Review E 74 (2006) 056705.
[30] V. Sofonea, Finite-difference lattice Boltzmann approach to pressure-driven microchannel flow with variable temperature, Europhysics Letters 76 (2006) 829.
[31] S. Ansumali, I.V. Karlin, S. Arcidiacono, A. Abbas, N. Prasianakis, Hydrodynamics beyond Navier–Stokes: exact solution to the lattice Boltzmann hierarchy, Physical Review Letters 98 (2007) 124502.
[32] I.V. Karlin, S. Ansumali, Renormalization of the lattice Boltzmann hierarchy, Physical Review E 76 (2007) 025701. R.
[33] L. Zheng, B.C. Shi, Z.H. Cai, Lattice Boltzmann method for simulating the temperature jump and velocity slip in microchannels, Communications in Computational Physics 2 (2007) 1125.
[34] S.H. Kim, H. Pitsch, I.D. Boyd, Slip velocity and Knudsen layer in the lattice Boltzmann method for microscale flows, Physical Review E 77 (2008) 026704.
[35] L. Zheng, Z.L. Guo, B.C. Shi, Discrete effects on thermal boundary conditions for the thermal latttice Boltzmann method in simulating microscale gas flows, Europhysics Letters 82 (2008) 44002.
[36] J.C. Maxwell, On stresses in rarified gases arising from inequalities of temperature, Philosophical Transactions of The Royal Society of London 170 (1879) 231.
[37] M. Smoluchowski, Über Wärmeleitung in verdünnten Gasen, Annalen der Physik und Chemie 64 (1898) 101.
[38] M. Watari, M. Tsutahara, Two-dimensional thermal model of the finite-difference lattice Boltzmann method with high spatial isotropy, Physical Review E 67 (2003) 036306.
[39] R.J. LeVeque, Numerical Methods for Conservation Laws, Birkhäuser, Basel, 1992.
[40] E.F. Toro, Riemann Solvers and Numerical Methods for Fluid Dynamics, Second ed., Springer, Berlin, 1999.
[41] A. Cristea, V. Sofonea, Two component lattice Boltzmann model with flux limiters, Central European Journal of Physics 2 (2004) 382.
[42] V. Sofonea, A. Lamura, G. Gonnella, A. Cristea, Finite-difference lattice Boltzmann model with flux limiters for liquid–vapor system, Physical Review E 70 (2004) 046702.
[43] G. Gonnella, A. Lamura, V. Sofonea, Lattice Boltzmann simulation of thermal nonideal fluids, Physical Review E 76 (2007) 036703.
[44] X. He, S. Chen, G.D. Doolen, A novel thermal model for the lattice Boltzmann method in incompressible limit, Journal of Computational Physics 146 (1998) 282.
[45] Y. Peng, C. Shu, Y.T. Chew, Simplified thermal lattice Boltzmann model for incompressible thermal flows, Physical Review E 68 (2003) 026701.
[46] Y. Peng, C. Shu, Y.T. Chew, A 3D incompressible thermal lattice Boltzmann model and its application to simulate natural convection in a cubic cavity, Journal of Computational Physics 193 (2004) 260.
[47] Y. Shi, T.S. Zhao, Z.L. Guo, Thermal lattice Bhatnagar–Gross–Krook model for flows with viscous heat dissipation in the incompressible limit, Physical Review E 70 (2004) 066310.
[48] H. Chen, X. Shan, Fundamental conditions for N-th-order accurate lattice Boltzmann models, Physica D (2008) 2003.
[49] N. Cao, S. Chen, S. Jin, D. Martinez, Physical symmetry and lattice symmetry in the lattice Boltzmann method, Physical Review E 55 (1997) R21.
[50] Y. Chen, H. Ohashi, M. Akiyama, Prandtl number of lattice Bhatnagar–Gross–Krook fluid, Physics of Fluids 7 (1995) 2280.
[51] M. Soe, G. Vahala, P. Pavlo, L. Vahala, H.D. Chen, Thermal lattice Boltzmann simulations of variable Prandtl number turbulent flows, Physical Review E 57 (1998) 4227.
[52] N.I. Prasianakis, I.V. Karlin, Lattice Boltzmann method for thermal flow simulation on standard lattices, Physical Review E 76 (2007) 016702.
[53] S. Ansumali, S. Arcidiacono, S.S. Chikatamarla, N.I. Prasianakis, A.N. Gorban, I.V. Karlin, Quasi-equilibrium lattice Boltzmann method, European Physical Journal B 56 (2007) 135.
[54] X.W. Shan, H. Chen, A general multiple-relaxation time Boltzmann collision model, International Journal of Modern Physica C 18 (2007) 635.
[55] N.I. Prasianakis, K.B. Boulouchos, Lattice Boltzmann method for simulation of weakly compressible flows at arbitrary Prandtl number, International Journal of Modern Physica C 18 (2007) 602.
[56] Q. Li, Y.L. He, Y. Wang, W.Q. Tao, Coupled double-distribution-function lattice Boltzmann method for the compressible Navier–Stokes equations, Physical Review E 76 (2007) 056705.
[57] L. Zheng, B.C. Shi, Z.L. Guo, Multiple-relaxation-time model for the correct thermohydrodynamic equations, Physical Review E 78 (2008) 026705.
[58] M. Knudsen, Die Gesetze der Molecular Stromung und die inneren Reibungstromung der Gase durch Rohren, Annalen der Physik 29 (1909) 75.
[59] Y. Zhou, R. Zhang, I. Staroselsky, H. Chen, W.T. Kim, M.S. Jhon, Simulation of micro- and nano-scale flows via the lattice Boltzmann method, Physica A 362 (2006) 68.
[60] R. Zhang, X. Shan, H. Chen, Efficient kinetic method for fluid simulation beyond the Navier–Stokes equation, Physical Review E 74 (2006) 046703.
[61] S. Ansumali, I.V. Karlin, C.E. Frouzakis, K.B. Boulouchos, Entropic lattice Boltzmann method for microflows, Physica A 359 (2006) 289.
[62] C. Cercignani, Theory and application of the Boltzmann equation, Scottish Academic Press, Edinburgh, 1975.